

Aerodynamic effect of wind barriers and running safety of trains on high-speed railway bridges under cross winds

Weiwei Guo^{*1,2,3}, He Xia^{1,2a}, Raid Karoumi^{3b}, Tian Zhang⁴ and Xiaozhen Li⁵

¹School of Civil Engineering, Beijing Jiaotong University, Beijing 100044, China

²Beijing Key Laboratory of Structural Wind Engineering and Urban Wind Environment, Beijing 100044, China

³Division of Structural Engineering and Bridges, KTH Royal Institute of Technology, SE-10044, Sweden

⁴Institute of Road and Bridge Engineering, Dalian Maritime University, Dalian 116026, China

⁵School of Civil Engineering, Southwest Jiaotong University, Chengdu 610031, China

(Received November 5, 2014, Revised December 29, 2014, Accepted January 8, 2015)

Abstract. For high-speed railways (HSR) in wind prone regions, wind barriers are often installed on bridges to ensure the running safety of trains. This paper analyzes the effect of wind barriers on the running safety of a high-speed train to cross winds when it passes on a bridge. Two simply-supported (S-S) PC bridges in China, one with 32 m box beams and the other with 16 m trough beams, are selected to perform the dynamic analyses. The bridges are modeled by 3-D finite elements and each vehicle in a train by a multi-rigid-body system connected with suspension springs and dashpots. The wind excitations on the train vehicles and the bridges are numerically simulated, using the static tri-component coefficients obtained from a wind tunnel test, taking into account the effects of wind barriers, train speed and the spatial correlation with wind forces on the deck. The whole histories of a train passing over the two bridges under strong cross winds are simulated and compared, considering variations of wind velocities, train speeds and without or with wind barriers. The threshold curves of wind velocity for train running safety on the two bridges are compared, from which the windbreak effect of the wind barrier are evaluated, based on which a beam structure with better performance is recommended.

Keywords: high-speed railway; cross winds; dynamic analysis; simply-supported beam bridge; wind barrier; windbreak effect; running safety

1. Introduction

With the development of high-speed railways, the running safety of train vehicles on bridges receives more attention than ever. A bridge built in a wind prone region may experience considerable deformation and low frequency vibration due to wind actions, which not only directly affects the working state and serviceability of the bridge, but also makes worse the running stability and safety of the train on the bridge (Xu *et al.* 2004, Li *et al.* 2005, Guo *et al.* 2007, Xia *et al.* 2008). Wind excitations on the train may directly induce its vehicles to vibrate and even to

*Corresponding author, Associate Professor, E-mail: wwguo@bjtu.edu.cn

^a Professor, E-mail: hxia88@163.com

^b Professor, E-mail: raid.karoumi@byv.kth.se

overturn or derail when the wind is strong (Cooper 1981, Baker 1991). Meanwhile, the vehicle vibration will be transferred through the wheels to the deck and further exaggerate the bridge vibration, which may in turn magnify the vibration of the vehicle on the bridge. Specially, when a train passes over the bridge at certain speed, the lateral wind pressure on the vehicles may form a lateral moving load series acting on the bridge. In this case, even the static wind forces due to the mean wind may induce dynamic responses of the bridge (Xia *et al.* 2006).

In some strong wind regions, wind barriers are required in the design of HSR bridges to assure the running safety and riding comfort of the train (Fujii *et al.* 1999, Noguchi *et al.* 2000). Wind barriers can reduce the aerodynamic forces on the train, but they also have negative influence on the bridge because they enlarge the windward area of the structure. Meanwhile, the existence of wind barriers exerts a disturbance on the wind field and increases turbulence effects, making the wind field around the bridge structure more complex. The wind loads on the train-bridge system with wind barriers are much different from those without barriers, therefore, the effect of wind barriers on the dynamic behavior of a coupled train-bridge system should be studied and evaluated.

Many efforts have been made to investigate the effect of cross winds on the train vehicles and their dynamic behaviors on embankments or bridges by wind tunnel tests (Kwon *et al.* 2001, Suzuki *et al.* 2003, Sanquer *et al.* 2004, Bocciolone *et al.* 2008, Golovanevskiy *et al.* 2012, Li *et al.* 2013, Li *et al.* 2014), or numerical simulations (Khieret *et al.* 2000, Cheliet *et al.* 2010, Baker 2010). Some investigations were made to improve the protection of trains extremely exposed to strong wind gusts (Baker *et al.* 1992, Saito *et al.* 2006, Xiang *et al.* 2014). Furthermore, Strukelj *et al.* (2005) numerically studied the effects of wind barrier geometry on resulting wind forces on road vehicles. Kwon *et al.* (2011) and Kim *et al.* (2011) presented the design criteria required for wind barriers to protect road vehicles on an expressway under a high side wind. Kozmar *et al.* (2012) experimentally studied the sheltering efficiency of wind barriers on roadway bridges in a boundary layer wind tunnel. Most of the studies on effect of wind barriers, however, were concentrated on how to reduce the wind velocity, wind pressure or the tri-component coefficients of the vehicle and bridge. Only a few studies concerned on the effect of wind barriers on the dynamic responses of a high-speed train when it passes over a railway bridge by systematically considering the interaction among the strong cross winds, the moving train vehicles and the bridge structures (Guo *et al.* 2011, Zhang *et al.* 2013).

The HSR line between Lanzhou and Urumqi in northwest China, which was just opened on Dec. 26, 2014, passes through a region that suffers more from windstorm damage than almost anywhere else in the world, where the instantaneous wind velocity often reaches 40~50 m/s. Because these strong winds are the main natural disaster that affects the running safety of high-speed trains, wind barriers are required for bridge designs in this region. There are two types of S-S beam bridge adopted, one with 32 m PC box beams and the other with 16 m PC trough beams, which are commonly used for high-speed railways in China. Because it is the first time to design wind barriers for HSR bridges in China, the design has experienced a long period of time and with a lot of alternative schemes. The options include the single-side and the double-side structures, the curved and straight structures, with different height and porosity. Guo *et al.* (2011) and Zhang *et al.* (2013) successively performed a dynamic analysis on a high-speed train passing over the box-beam bridge without or with different barrier schemes. After aerodynamic selection and optimization, the barrier structure type was eventually determined. It is a bilateral straight steel structure with the height of 3.5 m and composed of columns and screens. The porosity rate of the screen is not uniform, with the value of 10% at the bottom 1.0 m, while 20% at the other part.

As the subsequent study, this paper investigates the dynamic behavior of a high-speed train to strong winds when it passes over the two bridges adopting the final barrier structure type, based on the wind-train-bridge interaction system. The attention will focus on the effect of the wind barrier on the running safety indices of the train vehicles, including derailment factors, offload factors, lateral wheel/rail forces and overturn factors. These indices will be compared for the first time when the train passes over the two bridges, as well as the bridge responses. Furthermore, the threshold curves of wind velocity for ensuring the safety of the train on the two bridges with or without barriers will be proposed, based on which the better performance beam structure type will be recommended.

2. Dynamic model of wind-train-bridge interaction system

The behavior of wind-train-bridge interaction system is a complex time-varying dynamic problem related to many interactive factors, which is generally solved by the computer simulation method based on a dynamic analysis model for the system. The analysis model can be regarded as an integrated big spatial dynamic system composed of two submodels, the train-bridge interaction model and the wind model.

2.1 Train-bridge interaction model

The vibrations of the train and the bridge interact on and inter-affect each other, forming a complicated coupled vibration system. During the past decades, a number of sophisticated models have been developed to investigate the dynamic interaction between the bridge and the moving train, and many useful results published (Yang and Yau 1997, Frýba 2001, Au *et al.* 2001, Song *et al.* 2003, Lou 2005, Lee *et al.* 2006, Wallin *et al.* 2011, Guo *et al.* 2012). The present analysis method is to establish two sets of equations of motion, one for the bridge and the other for the train vehicles, which are dynamically coupled with each other through the contact relationship between the wheels and the rails. To simplify the analysis but with enough accuracy, the following assumptions are adopted:

(1) Each vehicle in a train is represented by a multi-rigid-body system connected by suspension springs and dashpots. By assuming five DOFs to the car-body, five DOFs to each bogie, and three DOFs to each wheel-set, a 27-DOF vehicle model is established for a 4-axle vehicle, as shown in Figures 1-2.

(2) The bridge is represented by a 3-D finite element model. The displacements of the deck at any section are identified in terms of the lateral displacement Y_B , vertical displacement Z_B , and torsional displacement θ_B at the shear center of the cross-section (see Fig. 2).

(3) There is no relative displacement between the track and bridge deck.

(4) The close contact assumption is adopted both in normal and tangent wheel-rail interactions, and no elastic deformation is considered.

Based on the above assumptions and taking the track irregularities as the self-excitations, the equations of motion for the train-bridge system are derived, which are combined with the wind model in the later section. Detailed derivation can be found in the authors' previous work (Xia *et al.* 2011).

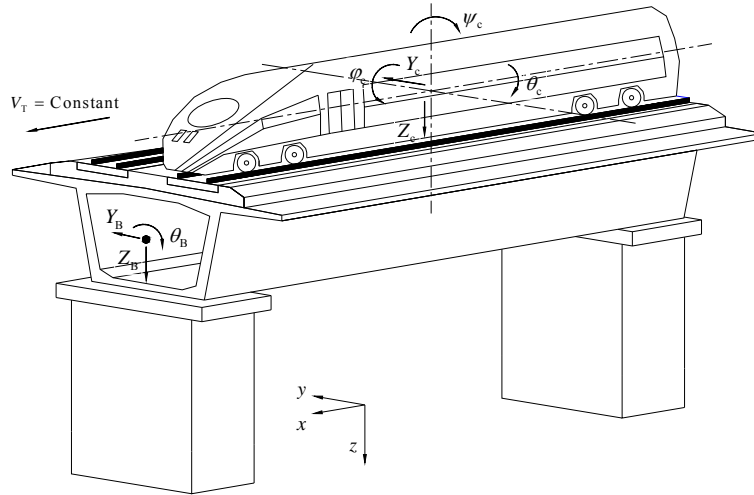


Fig. 1 Illustration of the train-bridge interaction model

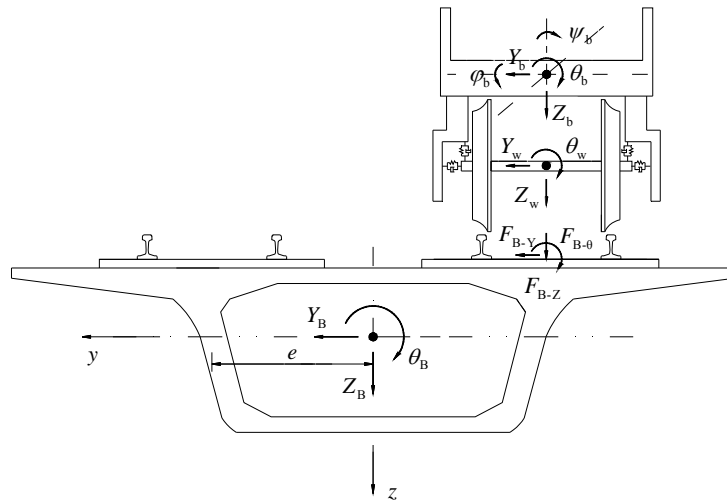


Fig. 2 Forces transmitted to the bridge deck through a wheel-set

2.2 Wind model

2.2.1 Simulation of stochastic wind velocity field

The wind velocity field of a bridge is a multidimensional, multivariate, homogeneous Gaussian stochastic process, since the wind velocity has three components of x , y , and z , and varies along the length of the deck. The computation is usually simplified as a combination of three independent, one-dimensional, multivariate stochastic processes, with the coherence between different dimensions ignored. When such a simplification is adopted and considering the train

moves on the deck of the bridge, the problem of simulating the wind velocity field will be concentrated on the generation of one-dimensional, i.e., in the y - z plane, multivariate stochastic processes.

There are several numerical methods for simulating stochastic wind velocity processes, such as the spectral representation method, the auto-regressive moving-average method, the covariance decomposition method, and so on. Herein, a fast spectral representation method based on explicitly expressing Cholesky's decomposition proposed by Cao *et al.* (2000) is adopted for the numerical simulation of the turbulent winds. This method assumes equi-elevation of the deck, equi-intervals of the wind velocity simulation points, and uniform distribution of the mean wind velocity and its spectrum along the deck. The time-histories of alongwind (y -direction) component $u_i(t)$ and upward wind (z -direction) component $w_i(t)$ at the i th simulation point can be generated by the following equations

$$\begin{cases} u_i(t) = \sqrt{2(\Delta\omega)} \sum_{m=1}^i \left[\sum_{k=1}^{N_f} \sqrt{S_u(\omega_{mk})} \times G_{im}(\omega_{mk}) \times \cos(\omega_{mk}t + \varphi_{mk}) \right] \\ w_i(t) = \sqrt{2(\Delta\omega)} \sum_{m=1}^i \left[\sum_{k=1}^{N_f} \sqrt{S_w(\omega_{mk})} \times G_{im}(\omega_{mk}) \times \cos(\omega_{mk}t + \varphi_{mk}) \right] \end{cases} \quad (1)$$

where $S_u(\omega_{mk})$ and $S_w(\omega_{mk})$ are, respectively, the alongwind and upward spectral density of the turbulent wind; N_f is the total number of frequency interval $\Delta\omega$ in the spectrum; $i=1,2,\dots,N$; N is the total number of wind velocity simulation points; φ_{mk} is a random variable uniformly distributed between 0 and 2π ; $G_{im}(\omega_{mk})$ is the correlation matrix between two different wind velocity points of i and m , which can be found in Cao *et al.* (2000).

2.2.2 Simulation of wind forces on bridge

The wind forces acting on the bridge deck consist of the steady-state force (\mathbf{F}_B^{st}) due to the mean wind, the buffeting force (\mathbf{F}_B^{bf}) due to the wind turbulence, while the self-exciting force due to the interaction between the bridge motion and wind velocity is neglected. Each force consists of three components of drag (D_B), lift (L_B) and rolling moment (M_B).

According to the classical airfoil theory, the steady wind force per unit deck length can be expressed as

$$\mathbf{F}_B^{\text{st}} = \begin{Bmatrix} D_B^{\text{st}}(x) \\ L_B^{\text{st}}(x) \\ M_B^{\text{st}}(x) \end{Bmatrix} = \frac{1}{2} \rho U^2 B \cdot \begin{bmatrix} (H/B)C_D(\alpha) \\ C_L(\alpha) \\ BC_M(\alpha) \end{bmatrix} \quad (2)$$

where ρ is the air density; U is the mean wind velocity; B and H are the width and height of the deck; $C_D(\alpha)$, $C_L(\alpha)$ and $C_M(\alpha)$ are, respectively, the static coefficients of drag, lift and moment; α is the angle of attack of normal incident wind referring to the horizontal plane of the deck.

The buffeting force per unit deck length can be expressed as (Simiu and Scanlan 1996)

$$\mathbf{F}_B^{\text{bf}} = \begin{Bmatrix} D_B^{\text{bf}}(x,t) \\ L_B^{\text{bf}}(x,t) \\ M_B^{\text{bf}}(x,t) \end{Bmatrix} = \frac{1}{2} \rho U^2 B \cdot \begin{Bmatrix} \frac{2C_D(\alpha)}{\bar{U}} u(t) + \frac{C'_D(\alpha)}{\bar{U}} w(t) \\ \frac{2C_L(\alpha)}{\bar{U}} u(t) + \frac{C'_L(\alpha) + C_D(\alpha)}{\bar{U}} w(t) \\ \frac{2BC_M(\alpha)}{\bar{U}} u(t) + \frac{BC'_M(\alpha)}{\bar{U}} w(t) \end{Bmatrix} \quad (3)$$

where $C'_D(\alpha)$, $C'_L(\alpha)$ and $C'_M(\alpha)$ are, respectively, the first derivatives of the drag, lift and moment coefficients at $\alpha=0$.

2.2.3 Simulation of wind forces on vehicle

The wind forces acting on a vehicle consist of the steady force (\mathbf{F}_V^{st}) and the buffeting force (\mathbf{F}_V^{bf}). The wind forces acting on the bogies and wheel-sets of the vehicle are neglected due to their small windward area, thus only those acting on the car-bodies are taken into account, which mainly refer to the drag (D_V), lift (L_V) and rolling moment (M_V) with respect to the mass center of the car-body, as shown in Fig. 3.

When a train runs at a constant speed V_T subjected to the instantaneous wind with the resultant velocity of V_W and the wind attack angle of α , the wind velocity relative to the train speed and its yaw angle φ are expressed as

$$V_R = \sqrt{V_W^2 + V_T^2} = \sqrt{[(U+u)^2 + w^2] + V_T^2} \quad (4)$$

$$\varphi = \arctan\left(\frac{\sqrt{(U+u)^2 + w^2}}{V_T}\right) \approx \arctan\left(\frac{U}{V_T}\right) \quad (5)$$

The steady wind force acting on the vehicle is only related to the mean part of oncoming wind components, which can be expressed as

$$\mathbf{F}_V^{\text{st}} = \begin{Bmatrix} D_V^{\text{st}} \\ L_V^{\text{st}} \\ M_V^{\text{st}} \end{Bmatrix} = \frac{1}{2} \rho A (U^2 + V_T^2) \cdot \begin{Bmatrix} C_D(\varphi) \\ C_L(\varphi) \\ HC_M(\varphi) \end{Bmatrix} \quad (6)$$

where A and H are the windward area and the height of car-body, respectively; $C_D(\varphi)$, $C_L(\varphi)$ and $C_M(\varphi)$ are, respectively, the aerodynamic drag, lift and moment coefficients of vehicle.

Owing to the unstable feature of the wind, a vehicle may also be affected by buffeting wind forces. In this paper, the buffeting wind forces induced by turbulent winds are calculated in the following way: First, the buffeting wind forces at different points along the bridge are simulated, with some of them at the bridge nodes and some at the points out of the bridge. Second, when a vehicle is between any of two adjacent points, its buffeting wind force can be obtained by the numerical interpolation of those at the two points, by assuming the same spatial correlation between the turbulent winds along the bridge and that along the train.

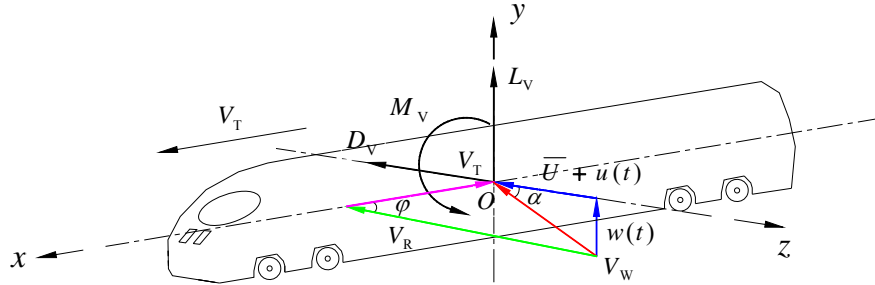


Fig. 3 Wind forces acting on the car-body of a vehicle

2.3 Coupled equations of motion for wind-train-bridge interaction system

By combining the train-bridge model and the wind model, the coupled equations of motion for the wind-excited train-bridge system can be obtained. To reduce the computational efforts efficiently, the modal superposition technique is adopted to solve the equation of motion of the bridge. It is assumed that only the first N modes of the bridge contribute to the interaction computation and the modal vectors are normalized to the mass matrix. The equations of motion of the system can thus be expressed as

$$\begin{cases} \mathbf{M}_V \ddot{\boldsymbol{\delta}}_V + \mathbf{C}_V \dot{\boldsymbol{\delta}}_V + \mathbf{K}_V \boldsymbol{\delta}_V = \mathbf{F}_V + \mathbf{F}_V^{st} + \mathbf{F}_V^{bf} \\ \ddot{\mathbf{q}} + \boldsymbol{\Phi}^T \mathbf{C}_B \boldsymbol{\Phi} \dot{\mathbf{q}} + \boldsymbol{\Phi}^T \mathbf{K}_B \boldsymbol{\Phi} \mathbf{q} = \boldsymbol{\Phi}^T (\mathbf{F}_B + \mathbf{F}_B^{st} + \mathbf{F}_B^{bf}) \end{cases} \quad (7)$$

where the subscripts V and B denote, respectively, the vehicle and the bridge; $\boldsymbol{\delta}$, $\dot{\boldsymbol{\delta}}$, and $\ddot{\boldsymbol{\delta}}$ are the displacement, velocity and acceleration vectors of the vehicles, respectively, and \mathbf{M}_V , \mathbf{C}_V and \mathbf{K}_V are the mass, damping and stiffness matrices; \mathbf{q} , $\dot{\mathbf{q}}$, and $\ddot{\mathbf{q}}$ are, respectively, the displacement, velocity and acceleration vectors of the bridge in modal coordinates, and $\boldsymbol{\Phi}$ is the mode shape matrix; \mathbf{C}_B and \mathbf{K}_B are, respectively, the damping and stiffness matrices of the bridge; \mathbf{F}_V and \mathbf{F}_B are the force vectors due to the interaction at the wheel/rail interfaces. Detailed information can be found in Xia *et al.* (2011).

Eq. (7) is actually a second order linear non-homogeneous differential equation with time-varying coefficients, which is solved using the Newmark implicit integral algorithm with $\beta=0.25$ and $\gamma=0.5$ according to the trapezoidal rule.

3. Case study

3.1 Engineering background

The high-speed railway line between Lanzhou and Urumqi in northwest China was just opened to service on Dec. 26, 2014, which passes through one of the most severe regions suffering from windstorm damage in the world, see Fig. 4. The total length of the HSR line in the wind region is

about 420 km. According to the Tiequan West measurement record in this area, there are more than 4 hours per day with the mean wind velocity higher than 20 m/s, and the maximum gust wind velocity is as high as 50 m/s.

There are 103 elevated bridges located in the wind region with the total length of 51.715 km. The design speed of the train vehicles on the bridges is 250 km/h. To ensure the running safety of the high-speed train on the bridges, the wind barriers are required and their windbreak effects should be evaluated.

3.2 Description of the bridge and train

As an illustrative case study, a S-S PC box-beam bridge with the span length of 32 m and a S-S PC trough-beam bridge with the span length of 16 m, which are widely used in the windy zones, are selected to perform the dynamic analysis. As shown in Fig. 5, the width and height of the box section are 12.7 m and 3.05 m, respectively. For the trough-beam bridge, the separated double U-shape girders are used, with the total width and height of 14.2 m and 2.0 m, respectively. Single-column piers and three-column piers are, respectively, adopted for the box-beam and the trough-beam, with the same height of 15 m (refer to Fig. 9).

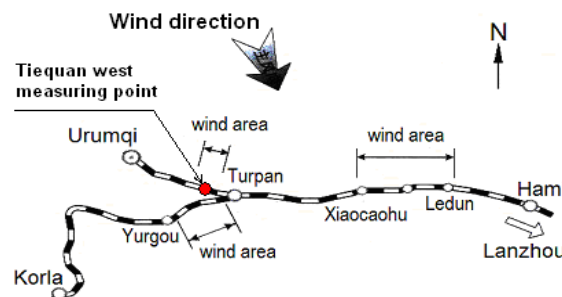


Fig. 4 Distribution of wind area in the Lanzhou-Urumqi HSR

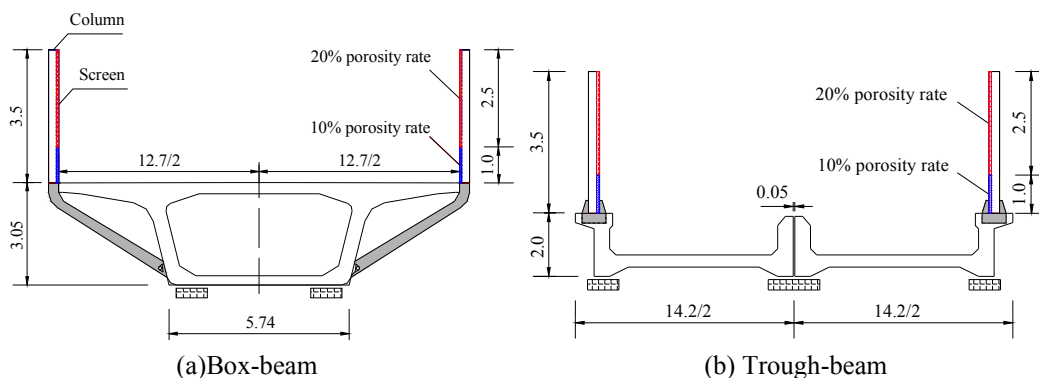


Fig. 5 The cross sections of the beams with the wind barrier (unit: m)

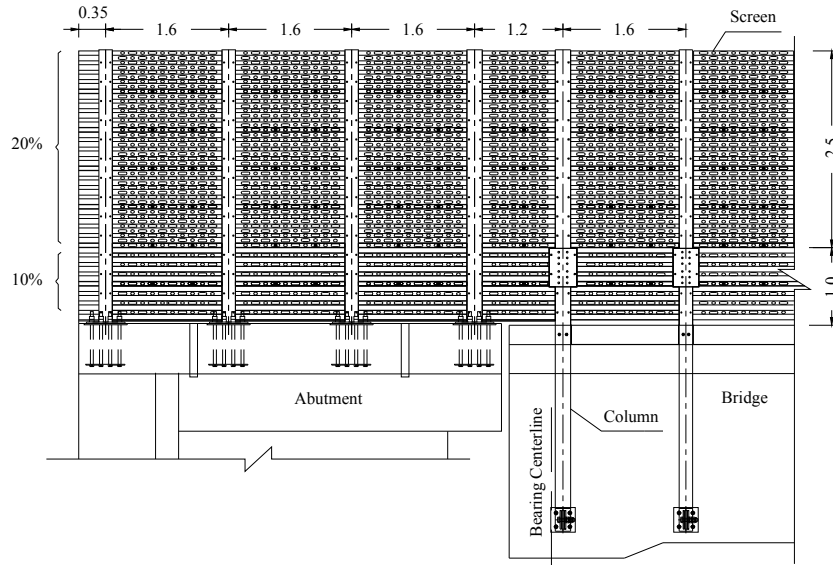


Fig. 6 Illustration of wind barrier on the bridge (unit: m)

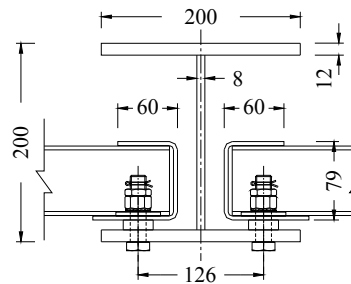


Fig. 7 Connections between the column and the screen (unit: mm)

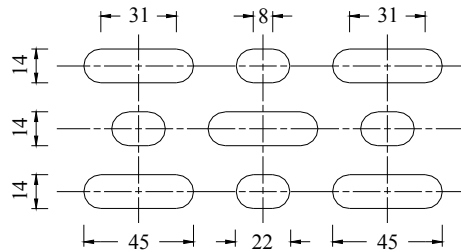


Fig. 8 Illustration of holes shape and size of the screen (unit: mm)

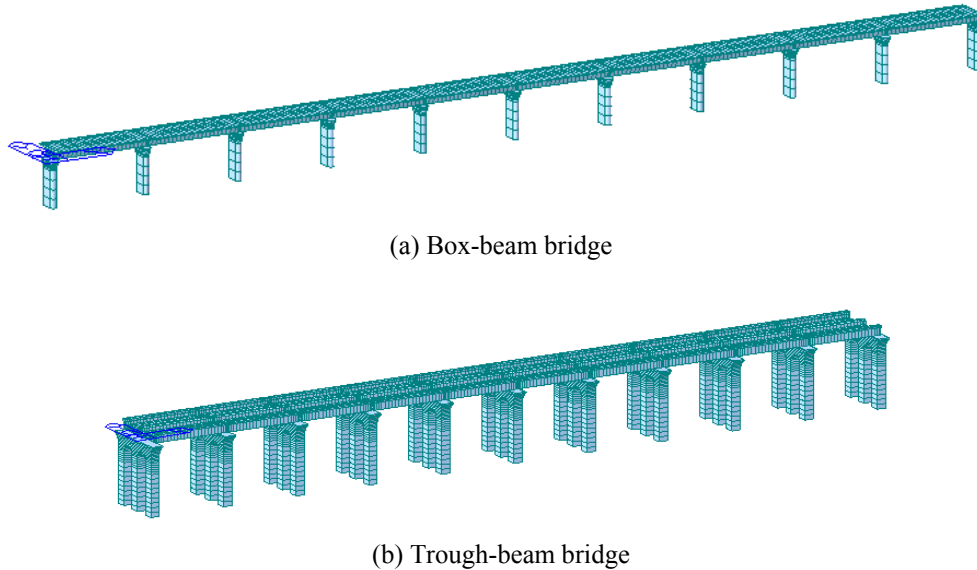


Fig. 9 The 3-D FE models of the two studied bridges

A bilateral straight steel wind barrier with the height of 3.5 m was designed for the two bridges, which is composed of columns and screens, as shown in Figs. 5-8. The columns, using the hot-rolled H-shape steel (Fig. 7), are fixed inside the beam by the embedded bolts. The screens with the thickness of 4 mm are connected with the columns also by bolts. The porosity rate of the screen is 10% at the bottom 1.0 m, while 20% at the other part. The holes shape and size of the screen are displayed in Fig. 8.

The two S-S bridges are modeled with ten identical spans to consider the multi-span effect. Since the stiffness of the barrier is much smaller than that of the bridge, and only the columns are connected with the beams directly, the barrier structures are not included in the bridge FE model (see Fig. 9).

By the FEM analysis, the natural vibration characteristics including frequencies and mode shapes of the two bridges are obtained. The fundamental frequencies in the lateral and vertical directions are, respectively, 3.274 Hz and 4.154 Hz for the box-beam bridge, and 4.451 Hz and 8.412 Hz for the trough-beam bridge, as shown in Table 1. To include the effects of the global deformation of the bridge, the first 80 modes up to a natural frequency of 31.887 Hz are taken in the dynamic analysis for the box-beam bridge, while the first 114 modes up to 31.630 Hz for the trough-beam bridge.

The track on the bridge is a ballast track. Because no measurement data are available for this new HSR, the lateral, vertical, and rotational track irregularities are taken into consideration by using the measured data from one of the main railways in China. The length of the data is 2,600 m with 8536 data points, including four groups of irregularities, i.e., left vertical, right vertical, left lateral and right lateral, used for the left and right rails. The statistical characteristic values are listed in Table 2. It can be seen that the maximum vertical and lateral amplitudes are 4.89 mm and 5.5 mm, respectively.

Table 1 Calculated natural frequencies of the two bridges

Modes	Frequency (Hz)	
	Box-beam bridge	Trough-beam bridge
1 st lateral bending mode	3.274	4.451
2 nd lateral bending mode	3.371	4.512
3 rd lateral bending mode	3.532	4.614
1 st vertical bending mode	4.154	8.412
2 nd vertical bending mode	4.436	8.426
3 rd vertical bending mode	4.443	8.447

Table 2 Statistical characteristics of measured irregularities

Values (mm)	Vertical		Lateral	
	Left	Right	Left	Right
maximum	4.89	4.61	5.06	5.4
minimum	-3.85	-4.25	-4.52	-5.5

Table 3 Fitted parameters for the irregularity spectra

Fitted parameters		<i>A</i>	<i>B</i>	<i>C</i>	<i>D</i>	<i>E</i>	<i>F</i>	<i>G</i>
Vertical	Left	1.1029	-1.4709	0.5941	0.8480	3.8016	-0.2500	0.0112
	Right	0.8581	-1.4607	0.5848	0.0407	2.8428	-0.1989	0.0094
Lateral	Left	0.2244	-1.5746	0.6683	-2.1466	1.7665	-0.1506	0.0052
	Right	0.3743	-1.5894	0.7265	0.4353	0.9101	-0.0270	0.0031
Torsional		0.1214	-2.1603	2.0214	4.5089	2.2227	-0.0396	0.0073

According to the measurement data, the irregularity spectra can be fitted as

$$S(f) = \frac{A(f^2 + Bf^3 + C)}{f^4 + Df^3 + Ef^2 + Ff + G} \tag{8}$$

where the unit of $S(f)$ is $\text{mm}^2/(1/\text{m})$; f is the spatial frequency of the track irregularities with the unit of $1/\text{m}$; A, B, C, D, E, F and G are the seven parameters to be fitted. The fitted parameters are listed in Table 3.



Fig. 10 Configuration of high-speed EMU train (unit: cm)

The train considered is a high-speed EMU train, with a composition of $4 \times (3M+1T)$, where M represents the motor-car and T the trailer-car. The full length, width and height of the carriages are 24.775 m, 2.7 m and 3.5 m, respectively, as shown in Fig. 10. The average static axle load is 160 kN for a motor-car and 146 kN for a trailer-car. Detailed information about the vehicle can be found in Xia *et al.* (2011).

3.3 Wind forces on the train-bridge system

The stochastic wind velocity fields are generated by Eq. (1). The alongwind and upward wind auto-spectra are adopted according to the Chinese Code

$$\begin{cases} S_u(\omega) = \frac{2\pi}{\omega} \cdot \frac{200f(z)u_*^2}{[1+50f(z)]^{5/3}} \\ S_w(\omega) = \frac{2\pi}{\omega} \cdot \frac{6f(z)u_*^2}{[1+4f(z)]^2} \end{cases} \quad (9)$$

$$f(z) = \frac{\omega z}{2\pi U_z} \quad (10)$$

$$u_* = \frac{0.4U_z}{\ln \frac{Z-H+2.5Z_0}{Z_0}} \quad (11)$$

where U_z is the mean wind velocity along the main windflow at height z ; u_* is the friction velocity of the wind; H is the average height of surrounding buildings; Z_0 is the ground roughness length.

The coherence function adopts the Davenport's form

$$\text{Coh}_{ij}(\omega) = \exp\left(-\lambda_{ij} \cdot \frac{\omega r_{ij}}{2\pi U_z}\right) \quad (12)$$

where r_{ij} is the distance between the two points i and j ; λ_{ij} is the coefficient relating to wind correlation, ranging from 7 to 12.

In total, there are 201 simulation points uniformly distributed along the deck axis with the distance of 5 m. The average elevation of the box deck and the trough deck are taken as 18.05 m and 15.75 m, respectively. The sampling frequency and duration used in the simulation of turbulent wind velocity are, respectively, 50 Hz and 10 min. The frequency interval and the time interval of wind velocity are, respectively, 0.001 Hz and 0.02 s.

Table 4 Tri-component coefficients and derivatives of the two beams

Item	Box-beam		Trough-beam	
	Without barrier	With barrier	Without barrier	With barrier
C_D	2.110	3.503	1.134	5.621
C_L	-0.202	0.055	-0.725	-0.316
C_M	-0.015	0.371	-0.137	0.210
C'_D	0.350	2.474	-7.733	-3.615
C'_L	-2.009	0.280	-3.252	0.827
C'_M	0.106	0.518	-0.686	-0.300

Table 5 Tri-component coefficients of vehicle on the beams

Item	Vehicle on box-beam		Vehicle on trough-beam	
	Without barrier	With barrier	Without barrier	With barrier
C_D	1.911	0.161	1.573	0.209
C_L	-0.001	0.022	0.012	0.002
C_M	1.173	0.144	0.898	0.160

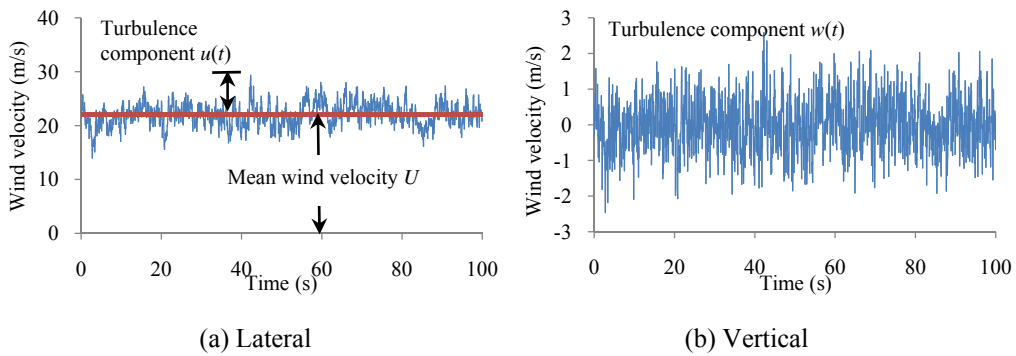


Fig. 11 Simulated instantaneous, mean and turbulence wind at the deck of box-beam bridge

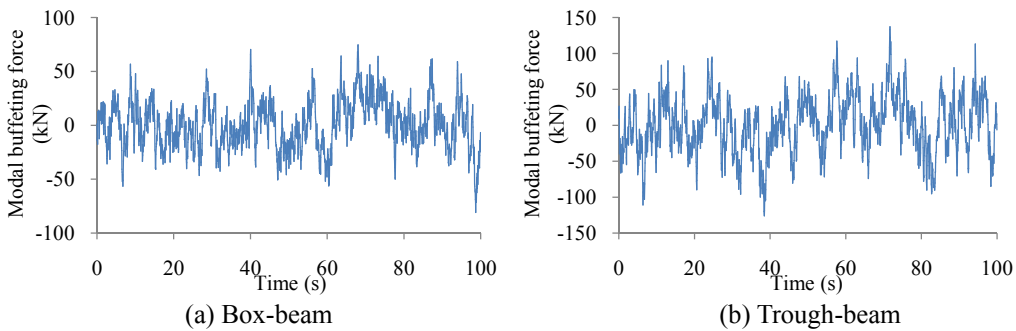


Fig. 12 Time history comparison of first modal buffeting drag force of the two bridges with barriers

The drag, lift, and moment coefficients of the train-bridge system were measured from wind tunnel tests. Table 4 displays the tri-component coefficients of the two beams and their first derivatives at the zero wind attack angle. The drag, lift, and moment coefficients of the vehicle on the two bridges with and without the barrier are listed in Table 5.

Fig. 11 shows the simulated time histories of lateral and vertical wind components at the deck of box-beam with respect to the instantaneous wind velocity of 30 m/s (the corresponding mean wind velocity is around 22 m/s). The buffeting forces acting on the bridge deck can be determined by Eq. (3) and the modal buffeting forces can then be obtained. Compared in Figs. 12 and 13 are the time histories of the first modal buffeting drag and lift forces on the two bridges with the barrier. It is seen that due to the larger drag and lift force coefficients, the modal buffeting drag and lift forces on the trough-beam with the barrier are larger than those on the box-beam with the barrier.

3.4 The TOM system during high wind period

Since the Lanzhou-Urumqi HSR passes through the severe windstorm regions, a TOM (Train Operation Management) system was established in the windy zone to ensure the running safety of trains on the bridges. The expected operating train speeds during high wind period were prescribed by ROD (the Railway Operation Department), as shown in Table 6. According to the provisions, the train should be able to run through the bridges at the design speed 250 km/h for the instantaneous wind velocity up to 30 m/s. For higher wind velocities, the train speed on the bridges should be limited. Specially, the railway operation should be closed when the wind velocity exceeds 40 m/s.

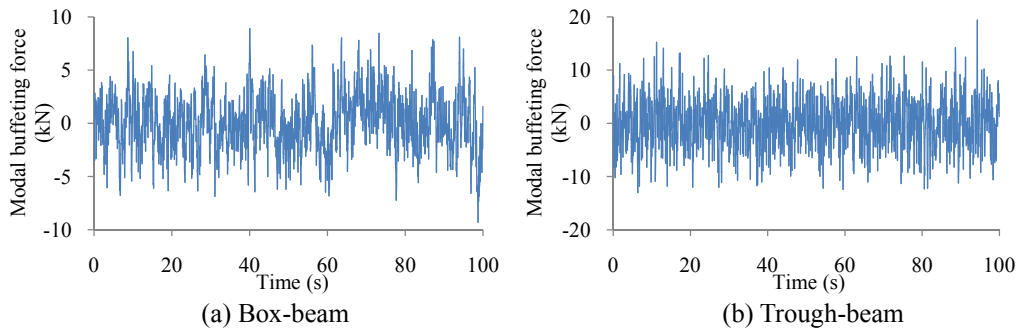


Fig. 13 Time history comparison of first modal buffeting lift force of the two bridges with barriers

Table 6 Operating train speed on the simply-supported bridges by ROD

Guideline	Instantaneous wind velocity $U+u(t)$			
	≤ 30 m/s	≤ 35 m/s	≤ 40 m/s	> 40 m/s
Train speed V_T	250 km/h	200 km/h	120 km/h	No entry

3.5 Dynamic responses of train vehicles

With the above bridge, train, track irregularity and wind load parameters, the whole histories of the train travelling through the two bridges subjected to the cross wind are simulated. The damping ratio of the bridge structure is taken as 2.5% for all modes in reference of the measured value (Luo 2005), and the integration time step is taken as 0.002 s to provide enough accuracy.

Displayed in Figs. 14 and 15 are the comparisons of the first vehicle acceleration time histories, when it runs at 250 km/h on the two bridges with barriers under the instantaneous wind velocity of 30 m/s. The travelling time is defined as from the moment when the first car enters the bridge to the moment when the last one goes out the bridge completely. So the train travelling time through the two bridges are calculated as 10.45 s and 8.15 s, respectively. The numerical results show that the maximum lateral and vertical accelerations of the first car on the box-beam bridge are 0.451 m/s² and 0.618 m/s², while on the trough-beam bridge are 0.518 m/s² and 0.535 m/s², respectively.

To investigate the windbreak effect of the wind barrier, the vehicle accelerations when there is no wind barrier are calculated for comparison. Illustrated in Figs. 16 and 17 are the lateral and vertical maximum accelerations of all vehicles when they pass over the two bridges with and without barriers.

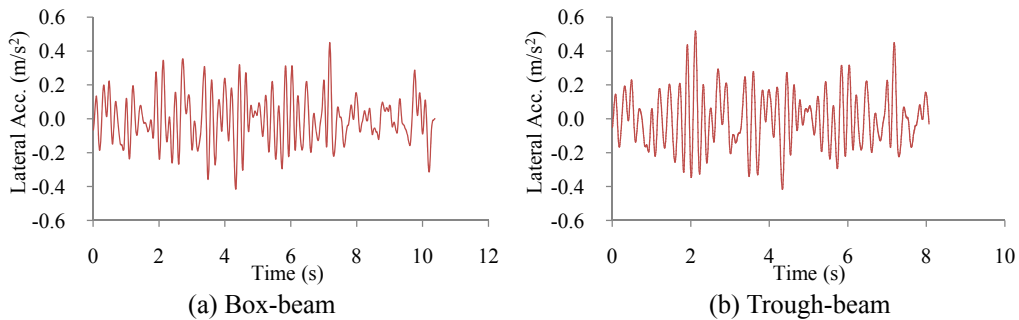


Fig. 14 Lateral acceleration time histories of the first car on bridges with wind barriers

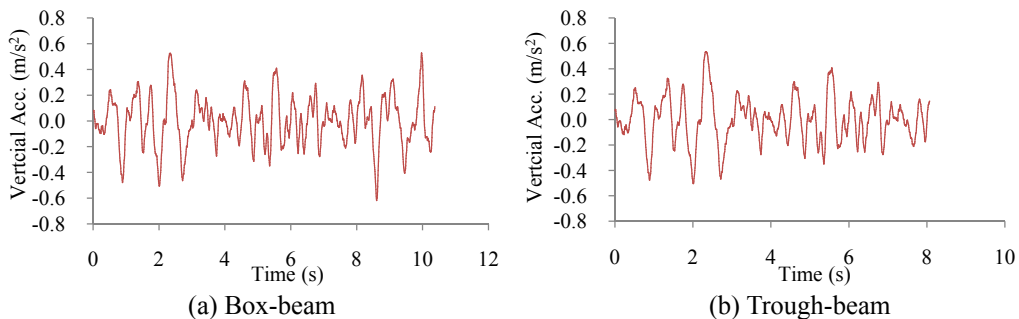


Fig. 15 Vertical acceleration time histories of the first car on bridges with wind barriers

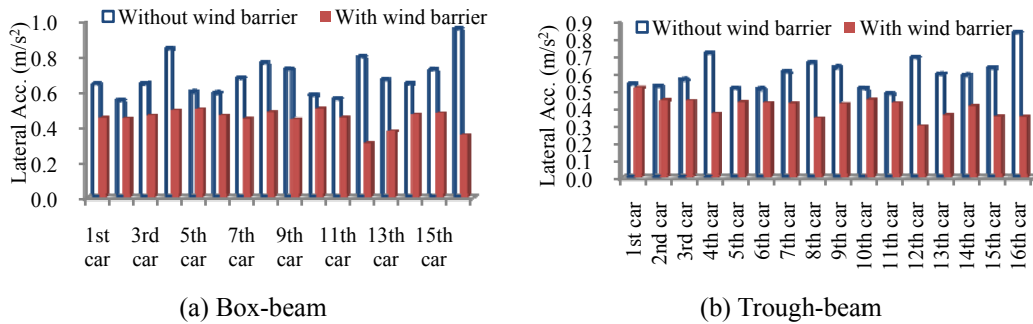


Fig. 16 Distribution of lateral acceleration of vehicles on bridges

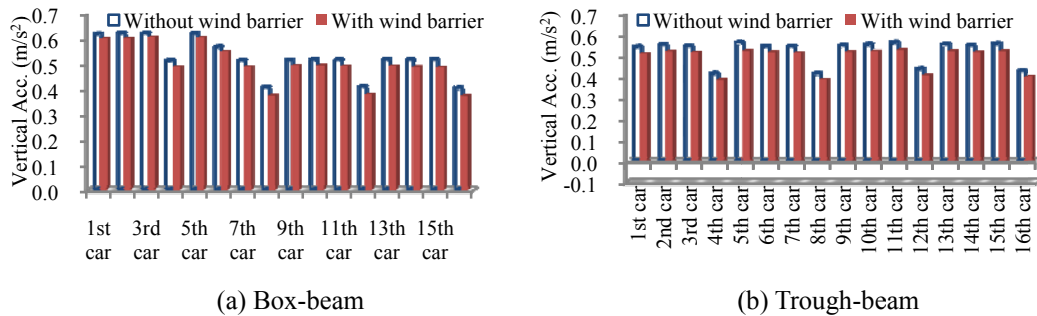


Fig. 17 Distribution of vertical acceleration of vehicles on bridges

It is seen from the figures that both the lateral and vertical accelerations of the vehicles are reduced due to the protection of the wind barriers. In general, the lateral accelerations decrease more obviously than the vertical one, because it is in the direction against the main wind flow. In the case without wind barrier, the maximum lateral accelerations of vehicle on the box-beam bridge and the trough-beam bridge are, respectively, 0.954 m/s^2 and 0.832 m/s^2 , both occurring at the last car. While in the case with wind barriers, the maximum vehicle lateral accelerations are reduced to 0.502 m/s^2 by 47% and 0.518 m/s^2 by 38%, respectively.

3.6 Running safety indices of train vehicles

The evaluation indices for the running safety of a train subjected to strong winds currently adopted in the HSR in China include: the derailment factor Q/P (defined as the ratio of the lateral force Q acting on the wheel-set to the total vertical force P acting on the same wheel-set at the climbing-up-rail side), the offload factor $\Delta P/P$ (defined as the ratio of the static and dynamic vertical force difference ΔP to the total vertical force P acting on the wheel-set), the lateral wheel force Q , and the overturn factor D (defined as the ratio of the overturn moment to the anti-overturn moment of the vehicle, which is induced by the direct wind actions on the car body). The allowable

values of these indices given in the Chinese codes are as follows (Ministry of Railways of PRC 2010)

$$\text{Derailment factor: } Q/P \leq 0.8 \tag{13a}$$

$$\text{Offload factor: } \Delta P/P \leq 0.6 \tag{13b}$$

$$\text{Lateral wheel force: } Q \leq 10 + P_0/3 \tag{13c}$$

$$\text{Overturn factor: } D \leq 0.8 \tag{13d}$$

where P_0 denotes the static wheel-set load in kN. In this case, the static loads of forces for the motor-car and trailer-car of the high-speed train are 160 kN and 146 kN, corresponding to their allowable lateral wheel forces of 63.3 kN and 58.7 kN, respectively.

By keeping the train speed at 250 km/h, while changing the instantaneous wind velocity from 0 m/s (without wind action) to 50 m/s, the distributions of the running safety indices of the train versus the wind velocity are calculated, as displayed in Figs. 18-22, in which the horizontal solid lines are the corresponding allowances.

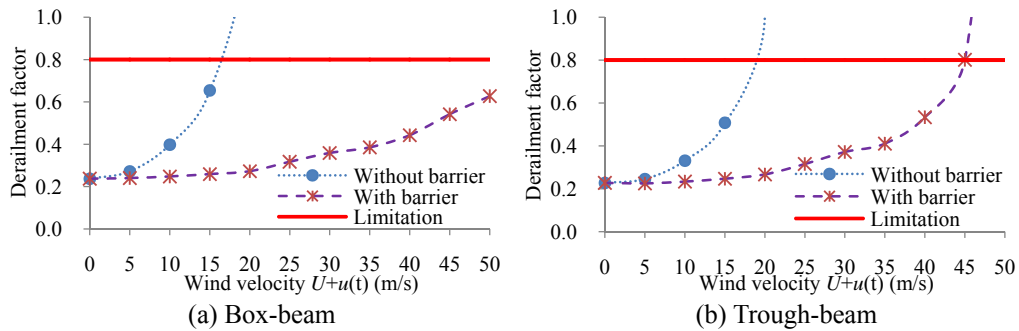


Fig. 18 Distributions of maximum derailment factors of cars on bridges with/without wind barriers

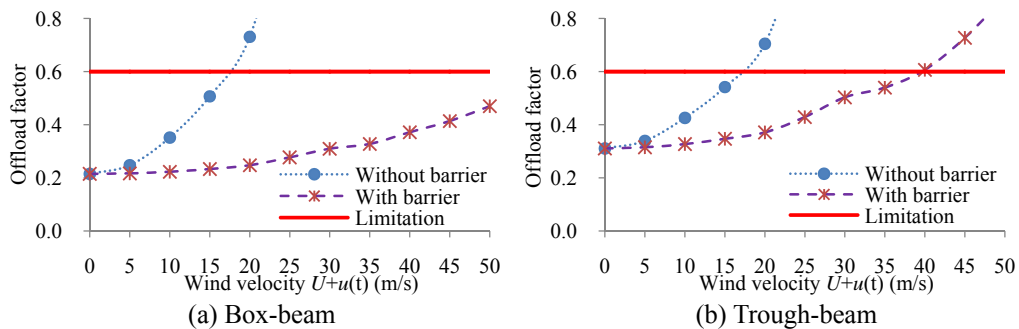


Fig. 19 Distributions of maximum offload factors of cars on bridges with/without wind barriers

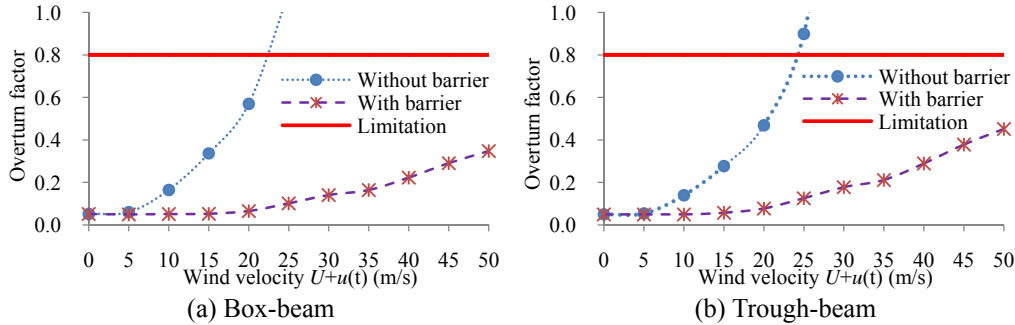


Fig. 20 Distributions of maximum overturn factors of cars on bridges with/without wind barriers

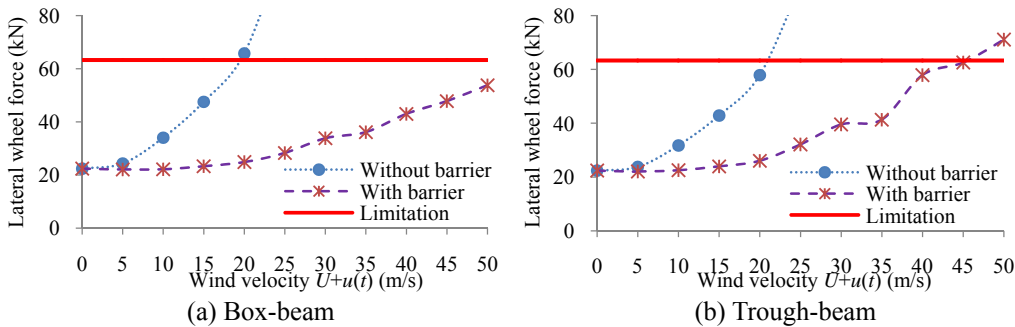


Fig. 21 Distributions of maximum lateral wheel forces of motor-cars on bridges with/without wind barriers

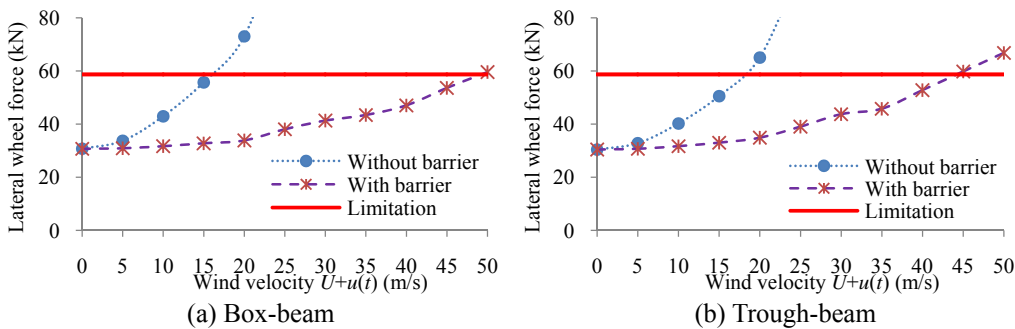


Fig. 22 Distributions of maximum lateral wheel forces of trailer-cars on bridges with/without wind barriers

It is seen that all the running safety indices of the train vehicles are sensitive to the wind velocity. In the case without wind barrier, the indices increase remarkably with wind velocity, while with barriers, the growth rate becomes less remarkable. The distribution curves show that the running safety of the train is greatly enhanced due to the windbreak effects of the wind barriers. The following characteristics can be summarized from the figures:

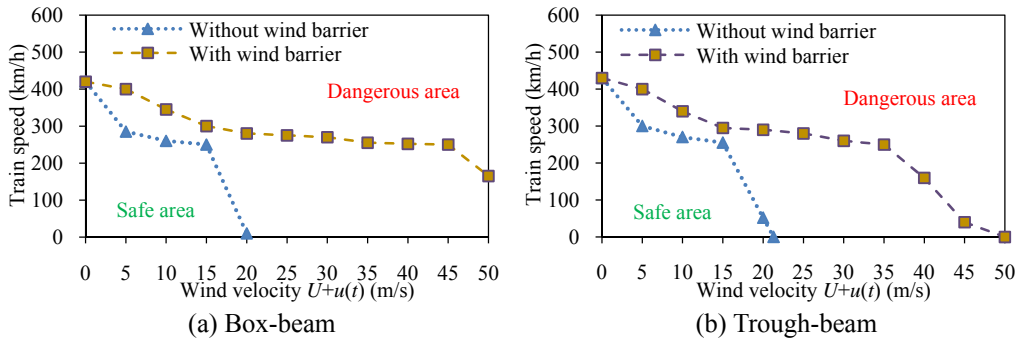


Fig. 23 Critical train speed for running safety vs instantaneous wind velocity

(1) For the box-beam bridge without wind barrier, when the train runs at the speed of 250 km/h, the lateral wheel force of the trailer-car goes beyond the limit first when the wind velocity is over 15 m/s, becoming the controlling index for the critical wind velocity to this train speed. As a contrast, in the case with the designed barrier, the critical wind velocity ensuring the train safety increases up to 45 m/s.

(2) For the trough-beam bridge, in the case without wind barrier, the critical wind velocity is also 15 m/s corresponding to the train speed of 250 km/h, but the controlling index is the offload factor. With the designed barrier, the critical wind velocity increases up to 35 m/s.

3.7 Critical train speed on bridge

In order to examine whether or not the designed wind barriers can satisfy the running safety requirement of the train on the two bridges according to the TOM system, the critical speeds of the train when it travels through the two bridges under various wind velocities are analyzed in the following way:

(1) Let the instantaneous wind velocity keep constant at each stage, the running safety indices of the train vehicles are calculated by changing the train speed. The critical speed of the train at which one of the running safety indices gets closest to but do not exceed its limit is obtained as the critical train speed related to this stage.

(2) Let the instantaneous wind velocity change from 0 m/s to 50 m/s with an increment of 5 m/s, the critical speeds of the train related to all stages are calculated.

(3) By plotting the calculated results in an identical coordinate system, with the abscissa representing the wind velocity and the ordinate the train speed, the relationship curves between the critical train speed and the wind velocity is obtained, as shown in Fig. 23.

It is easy to find that in the case without wind barrier, the critical speed of the train on the bridges decreases remarkably with increasing wind velocity and the TOM provisions cannot be satisfied once the wind velocity is higher than 15 m/s. While with the designed wind barriers, the critical train speed on both the two bridges are higher than the expected train speed, indicating that the provisions can be fully guaranteed. For the wind velocity lower than 35 m/s, the critical train speeds on the two bridges are close to each other. However, for the wind velocity higher than 35 m/s, the critical speed of the train on the trough-beam bridge drops off remarkably. For the wind

velocity higher than 45 m/s, the rail traffic on the trough-beam bridge should be closed. As a contrast, even when the wind velocity reaches 50 m/s, the train can still run safely at 165 km/h on the box-beam bridge. According to the measured data from the wind tunnel test, it is seen that the drag, lift and moment coefficients for the trough-beam are larger than those for the box-beam in the case with barriers. Besides, the drag and moment coefficients for the vehicle on the trough-beam are also larger than on the box-beam, as shown in Tables 4 and 5. Thus for the box-beam bridge, the wind loads on the vehicle and bridge are smaller under the same wind velocity due to its good aerodynamic characteristics, which leads to the two structures behave so different.

3.8 Dynamic responses of bridge

Compared in Figs. 24 and 25 are, respectively, the time-histories of lateral and vertical displacements of the bridge decks at the 5th mid-span (displayed in the figures), when the train speed is 250 km/h and the instantaneous wind velocity is 30 m/s.

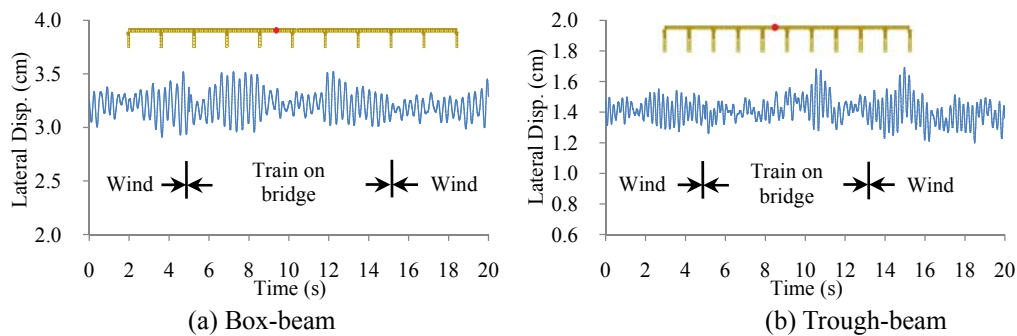


Fig. 24 Comparisons of lateral displacement time-histories of two bridges

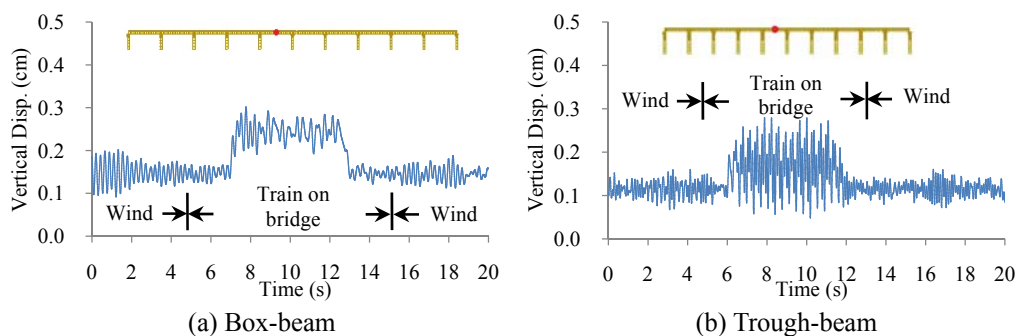


Fig. 25 Comparisons of vertical displacement time-histories of two bridges

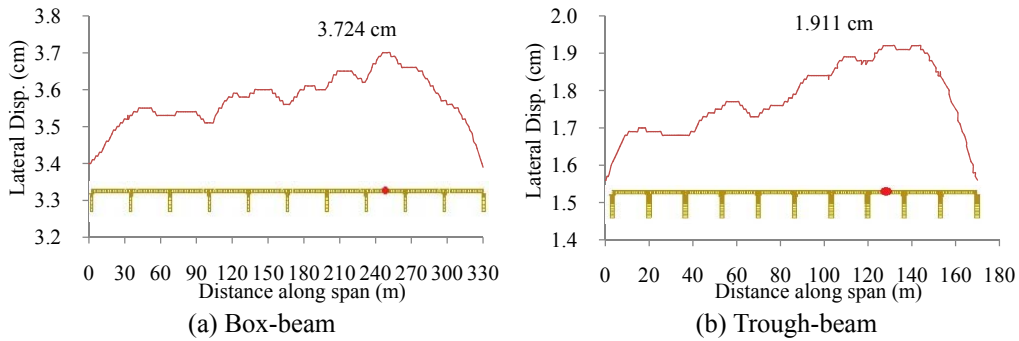


Fig. 26 Distribution of maximum lateral deck displacements along bridge span

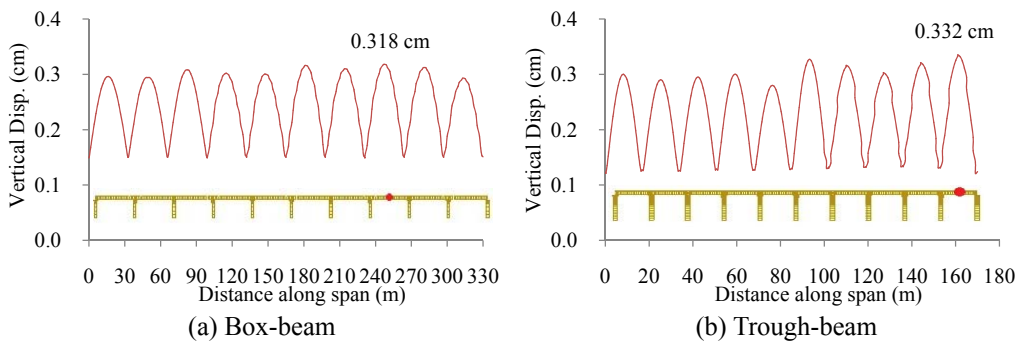


Fig. 27 Distribution of maximum vertical deck displacements along bridge span

It is seen that the maximum lateral and vertical displacement for the box-beam bridge are 3.521 cm and 0.302 cm, while for the trough-beam bridge are 1.690 cm and 0.279 cm, respectively. The static deformation of the bridge induced by the cross winds can be observed from the figures. The lateral static displacements for the box-beam and trough-beam bridges are 3.205 cm and 1.408 cm, while the vertical ones are 0.147 cm and 0.115 cm, respectively. Furthermore, one can find that the lateral response of the bridge is mainly influenced by the fluctuating winds, while the vertical response is mainly induced by the gravity loading of the train.

Compared in Figs. 26 and 27 are the distributions of maximum lateral and vertical deck displacements along the bridge span. It is seen that under the combined effect of the cross wind and the moving train, the lateral and vertical maximum deck displacements of the box-beam bridge both occur at the middle of the 8th span, with the value of 3.724 cm and 0.318 cm, respectively. The maximum lateral deck displacement of the trough-beam bridge also occurs at the middle of the 8th span and with the value of 1.911 cm, while the maximum vertical one occurs at the middle of the last span, with the value of 0.332 cm.

4. Conclusions

The dynamic responses of two multi-span S-S PC beam bridges with the wind barrier subjected to a high-speed train and strong cross winds are computed by using a wind-train-bridge system model. The whole histories of the train passing through two bridges are simulated under several loading cases. The following conclusions have been obtained from the study:

- Protected by the wind barrier, the vehicle accelerations are efficiently reduced, and in general, the windbreak effect on the lateral acceleration is higher than on the vertical one, because the former is in the direction of the main wind flow.
- The running safety indices of the train are sensitive to the wind velocity, among which the offload factor and the lateral wheel force of the trailer-car are the key factors that control the train safety when it passes over the two bridges. In the case without wind barrier, all the indices increase remarkably with wind velocity, while comparatively slow in the case with the barriers. In the wind velocity range of 0 m/s ~ 40 m/s, the critical speeds of the train on the two bridges with the designed barriers are all higher than the expected ones, indicating that the TOM provisions can be guaranteed due to the protection of the wind barriers.
- In the wind velocity range of 0 m/s ~ 35 m/s, the critical speeds of the train on the two bridges are very close to each other. However, as the wind velocity exceeds 35 m/s, the critical speeds of the train on the trough-beam bridge drop off remarkably. Once the wind velocity exceeds 45 m/s, the rail traffic on the trough-beam bridge should be closed. As a contrast, even when the wind velocity reaches 50 m/s, the train can still run safely at 165 km/h on the box-beam bridge.
- The existence of the wind barriers brings negative effects to the bridge, because they increase the windward area of the structure. In the case with barriers, the lateral deflections to the span reach 1/859 for the box-beam bridge and 1/837 for the trough-beam bridge, while the vertical deflections to the span reach 1/10063 for the box-beam bridge and 1/4819 for the trough-beam bridge.
- With the designed wind barriers, the box-beam bridge has better performance than the trough-beam bridge in the windy zone of the Lanzhou-Urumqi HSR by comparing the running safety indices of the train vehicles as well as the bridge responses.

It is worthwhile to point out that the case study presented in this paper is just a single event. It is obviously insufficient for the optimization and selection of HSR bridge type in the windy zone. Therefore, further investigations on the relationship between the design details of the wind barrier and the dynamic behaviors of train-bridge system, more case studies and field measurement data are needed in the future before solid conclusions can be reached.

Acknowledgments

The research described in this paper was financially supported by the National Basic Research Program of China (“973” Project, Grant No. 2013CB036203), the National Natural Science Foundations of China (Grant No. 51308034, U1434205), and the “111” project of China (Grant No. B13002).

References

- Au, F.T.K., Cheng, Y.S. and Cheung, Y.K. (2001), "Effects of random road surface roughness and long-term deflection of prestressed concrete girder and cable-stayed bridges on impact due to moving vehicles", *Comput. Struct.*, **79**(8), 853-872.
- Baker, C.J. (1991), "Ground vehicles in high cross winds part1: steady aerodynamic forces", *J. Fluid. Struct.*, **5**(2), 69-90.
- Baker, C.J. and Reynolds, S. (1992), "Wind-induced accidents of road vehicles", *Accid. Anal. Prev.*, **24**(6), 559-575.
- Baker, C.J. (2010), "The simulation of unsteady aerodynamic cross wind forces on trains", *J. Wind Eng. Ind. Aerod.*, **98**(2), 88-99.
- Baker, C. (2010), "The flow around high speed trains", *J. Wind Eng. Ind. Aerod.*, **98**(6-7), 277-298.
- Bocciolone, M., Cheli, F., Corradi, R., Muggiasca, S. and Tomasini, G. (2008), "Crosswind action on rail vehicles: wind tunnel experimental analyses", *J. Wind Eng. Ind. Aerod.*, **96**, 584-610.
- Cao, Y.H., Xiang, H.F. and Zhou, Y. (2000), "Simulation of stochastic wind velocity field on long-span bridges", *J. Eng. Mech. - ASCE*, **126**(1), 1-6.
- Cheli, F., Ripamonti, F., Rocchi, D. and Tomasini, G. (2010), "Aerodynamic behaviour investigation of the new EMUV250 train to cross wind", *J. Wind Eng. Ind. Aerod.*, **98**(4-5), 189-201.
- Cooper, R.K. (1981), "The effect of cross winds on trains", *J. Fluid Mech.*, **103**(1), 170-178.
- Fryba, L. (2001), "A rough assessment of railway bridges for high speed trains", *Eng. Struct.*, **23**(5), 548-556.
- Fujii, T., Maeda, T., Ishida, H., Imai, T., Tanemoto, K. and Suzuki, M. (1999), "Wind-induced accidents of train/vehicles and their measures in Japan", *Quart. Report Railway Tech. Res. Inst.*, **40**(1), 50-55.
- Golovanevskiy, V.A., Chmovzh, V.V. and Girka, Y.V. (2012), "On the optimal model configuration for aerodynamic modeling of open cargo railway train", *J. Wind Eng. Ind. Aerod.*, **107-108**, 131-139.
- Guo, W.W., Xu, Y.L., Xia, H., Zhang, W.S. and Shum, K.M. (2007), "Dynamic response of suspension bridge to typhoon and trains II: numerical results", *J. Struct. Eng. - ASCE*, **133**(1), 12-21.
- Guo, W.W., Xia, H., Zhang, T. and Sun, G.J. (2011), "Dynamic responses of a railway bridge under high-speed trains subjected to turbulent winds", *Proceedings of the 8th International Conference on Structural Dynamics in Belgium*, Leuven, July, MS07-137.
- Guo, W.W., Xia, H., De Roeck, G. and Liu, K. (2012), "Integral model for train-track-bridge interaction on the Sesia Viaduct: dynamic simulation and critical assessment", *Comput. Struct.*, **112-113**, 205-216.
- Khier, W., Breuer, M. and Durst, F. (2000), "Flow structure around trains under side wind conditions: a numerical study", *Comput. Fluids*, **29**(2), 179-195.
- Kim, D.H., Kwon, S.D., Lee, I.K. and Jo, B.W. (2011), "Design criteria of wind barriers for traffic. Part 2: decision making process", *Wind Struct.*, **14**(1), 71-80.
- Kozmar, H., Procino, L., Borsani, A. and Bartoli, G. (2012), "Sheltering efficiency of wind barriers on bridges", *J. Wind Eng. Ind. Aerod.*, **107-108**, 274-284.
- Kwon, H.B., Park, Y.W., Lee, D.H. and Kim, M.S. (2001), "Wind tunnel experiments on Korean high-speed trains using various ground simulation techniques", *J. Wind Eng. Ind. Aerod.*, **89**(13), 1179-1195.
- Kwon, S.D., Kim, D.H., Lee, S.H. and Song, H.S. (2011), "Design criteria of wind barriers for traffic. Part 1: wind barrier performance", *Wind Struct.*, **14**(1), 55-70.
- Lee, C.H., Kawatani, M., Kim, C.W., Nishimura, N. and Kobayashi, Y. (2006), "Dynamic response of a monorail steel bridge under a moving train", *J. Sound Vib.*, **294**(3), 562-579.
- Li, Y.L., Qiang, S.Z., Liao, H.L. and Xu, Y.L. (2005), "Dynamics of wind-rail vehicle-bridge systems", *J. Wind Eng. Ind. Aerod.*, **93**(6), 483-507.
- Li, Y.L., Hu, P., Cai, C.S. and Qiang, S.Z. (2013), "Wind tunnel study of sudden change of vehicle wind loads due to windshield effects of bridge towers and passing vehicles", *J. Eng. Mech. - ASCE*, **139**(9), 1249-1259.
- Li, Y.L., Hu, P., Xu, Y.L., Zhang, M.J. and Liao, H.L. (2014), "Wind loads on a moving vehicle-bridge deck

- system by wind-tunnel model test”, *Wind Struct.*, **19**(2), 145-167.
- Lou, P. (2005), “vehicle-track-bridge interaction element considering vehicle’s pitching effect”, *Finite Elem. Anal. Des.*, **41**(4), 397-427.
- Ministry of Railways of PRC. (2010), *Code for design of high-speed railway TB 10621-2009*, China Railway Publishing House, Beijing (in Chinese).
- Noguchi, T. and Fujii, T. (2000), “Minimizing the effect of natural disasters”, *Jpn. Rail. Transport Rev.*, **23**, 52-59.
- Saito, H., Suzuki, M. and Tanemoto, M. (2006), “Effects of wind fences on aerodynamic characteristics of train/ vehicles in cross winds”, *Proceedings of the 6th Asia-Pacific Conference on Wind Engineering*, Seoul.
- Sanquer, S., Barre, C., De Virel, M.D. and Cleon, L.M. (2004), “Effect of cross winds on high-speed trains: development of a new experimental methodology”, *J. Wind Eng. Ind. Aerod.*, **92**(7-8), 535-545.
- Simiu, E. and Scanlan, R.H. (1996), *Wind Effects On Structures: Fundamentals And Applications To Design*, Wiley Publishing, New York.
- Song, M.K., Noh, H.C. and Choi, C.K. (2003), “A new three-dimensional finite element analysis model of high-speed train-bridge interactions”, *Eng. Struct.*, **25**(13), 1611-1626.
- Strukelj, A., Ciglaric, I. and Pipenbahr, M. (2005), “Analysis of a bridge structure and its wind barrier under wind loads”, *Struct. Eng. Int.*, **15**(4), 220-227.
- Suzuki, M., Tanemoto, K. and Maeda, T. (2003), “Aerodynamic characteristics of train/vehicles under crosswinds”, *J. Wind Eng. Ind. Aerod.*, **91**(1), 209-218.
- Wallin, J., Leander, J. and Karoumi, R. (2011), “Strengthening of a steel railway bridge and its impact on the dynamic response to passing trains”, *Eng. Struct.*, **33**, 635-646.
- Xia, H., Zhang, N. and Guo, W.W. (2006), “Analysis of resonance mechanism and conditions of train-bridge system”, *J. Sound Vib.*, **297**(3-5), 810-822.
- Xia, H., Guo, W.W., Zhang, N. and Sun, G.J. (2008), “Dynamic analysis of a train-bridge system under wind action”, *Comput. Struct.*, **86**(19-20), 1845-1855.
- Xia, H., De Roeck, G. and Goicolea, J.M. (2011), *Bridge Vibration And Controls: New Research*, Nova Science Publishers, New York.
- Xiang, H.Y., Li, Y.L., Chen, B. and Liao, H.L. (2014), “Protection effect of railway wind barrier on running safety of train under cross winds”, *Adv. Struct. Eng.*, **17**(8), 1177-1187.
- Xu, Y.L., Zhang, N. and Xia, H. (2004), “Vibration of coupled train and cable-stayed bridge system in cross wind”, *Eng. Struct.*, **26**(10), 1389-1406.
- Yang, Y.B. and Yau, J.D. (1997), “Vehicle-bridge interaction element for dynamic analysis”, *J. Struct. Eng. - ASCE*, **123**(11), 1512-1518.
- Zhang, T., Xia, H. and Guo, W.W. (2013), “Analysis on running safety of train on bridge with wind barriers subjected to cross wind”, *Wind Struct.*, **17**(3), 203-225.